Thermochimica Acta, 154 (1989) 13–25
Elsevier Science Publishers B.V., Amsterdam – Printed in The Netherlands

MICROCALORIMETRIC STUDY OF OXYGEN ADSORPTION ON GRAPHITE-SUPPORTED RHODIUM MICROCRYSTALS *

JONATHAN PHILLIPS ** and ROBERT R. GATTE

Department of Chemical Engineering, The Pennsylvania State University, 133 Fenske Laboratory, University Park, PA 16802 (U.S.A.)

(Received 12 December 1988)

ABSTRACT

A novel true differential calorimeter was used to measure the differential heat and kinetics of oxygen adsorption (approximately 300 K) on graphite-supported rhodium particles. The particle size distribution was determined using a transmission electron microscope and the phases of rhodium present were determined using X-ray diffraction. It was found that only true chemisorption occurs (not bulk oxidation), and that the differential heat of adsorption and the adsorption stoichiometry are a function of particle size. This is consistent with many earlier studies which show the catalytic behavior of rhodium particles to be dependent on size.

INTRODUCTION

The use of supported rhodium as a catalyst has received considerable attention in recent years [1–20]. Rhodium has been shown to be an important catalyst for several processes, including catalytic conversion of automotive exhaust (NO reduction, CO oxidation) [1,2] and synthesis gas conversion (Fischer–Tropsch synthesis) [3–7]. In the case of syngas conversion, rhodium is an interesting catalyst because of its ability to synthesize both hydrocarbons and oxygenated products. In addition, TiO_2-supported rhodium has displayed the classic strong metal support interaction (SMSI) behavior characteristic of the more noble Group VIII metals on this substrate [8,9]. All previous studies of supported rhodium particles have focused on the determination of particle size, shape and surface area. There is a need for techniques which can be used to establish the chemistry of the surface of supported rhodium microcrystals, because of their wide range of catalytic application and interesting chemical properties.

* Dedicated to Professor James J. Christensen in memory of his contribution to innovation in calorimetry.

** Author to whom correspondence should be addressed.

0040-6031/89/$03.50

This study was designed to investigate the chemistry of rhodium microcrystals using adsorption microcalorimetry. In brief, oxygen was differentially dosed onto graphite-supported rhodium particles and the heats and rates of adsorption were measured. Graphite was used as the support material because it is virtually inert [21–24]. This allows an analysis to be made of the behavior of the rhodium particles without the added complications associated with support interaction. From this study it can be seen that there are differences between rhodium bulk and surface chemistry, and it is clearly shown that the chemistry of rhodium particle surfaces is strongly dependent on particle size.

EXPERIMENTAL

Catalyst preparation

The catalyst sample was prepared by impregnation of GTA-grade Grafoil (Union Carbide Corp.) with an aqueous solution of $RhCl_3 \cdot xH_2O$. The Grafoil was finely ground and pretreated as described previously. Grafoil is a highly graphitic, very pure carbon, previously shown to have a relatively low average surface area of 22 $m^2\ g^{-1}$, nearly all of which exists as highly uniform basal plane surface [22,25,26].

The solution was prepared by dissolving 0.322 g of the rhodium salt (FW = 209.26) in 6.0 ml of distilled water, adding 6 drops of HCl to ensure that the salt was completely dissolved. Approximately 2.00 ml of the solution was added dropwise to approximately 1.00 g of Grafoil with constant stirring. This produced a catalyst with roughly 5.0 wt.% rhodium.

The sample was air dried for several days at room temperature, compacted and reflaked (to allow more catalyst to fit into the calorimeter sample cell) and then placed in the calorimeter pretreatment reactor.

Differential microcalorimetry

The design and operation of the differential adsorption microcalorimeter used for this study have been described elsewhere [27,28]. Briefly, the sample was reduced in the calorimeter pretreatment reactor at the temperature of interest (200 °C or 400 °C) in a hydrogen atmosphere prior to adsorption studies. Following this treatment, the sample was evacuated at the same temperature for at least 4 h (or until the calorimeter pressure heads indicated that the residual sample pressure was below 1×10^{-4} Torr) to remove the adsorbed hydrogen. Finally, the sample was allowed to cool and transferred into the sample cell. The entire calorimeter was then sealed in a constant temperature enclosure and allowed to equilibrate to 30 °C prior to

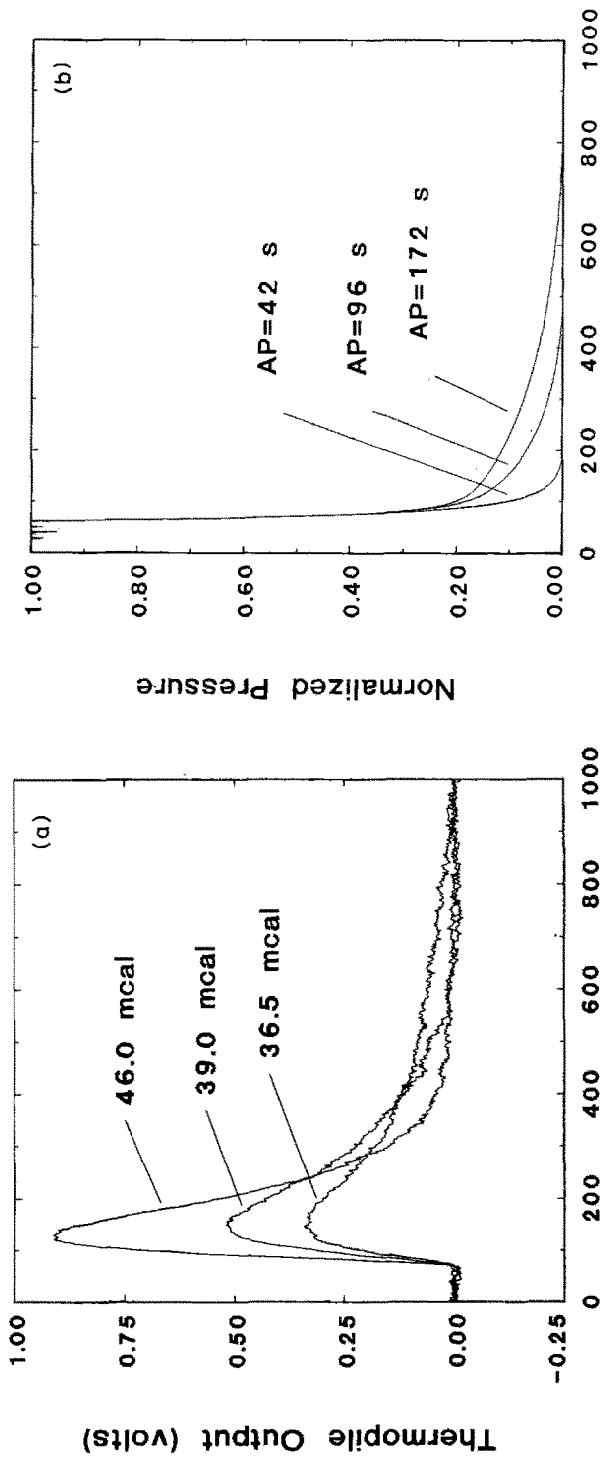

Fig. 1. Typical raw calorimeter data from oxygen adsorption on Rh–Grafoil. (a) Characteristic thermograms collected during doses near the boundary between regions I and II. The amount of heat evolved during each dose (i.e. the integrated area) is indicated. (b) Characteristic normalized pressure response curves. The rate of adsorption (t') is estimated by the time it takes to achieve a normalized pressure of 0.1 (adsorption parameter). A parameter called the normalized adsorption parameter (NAP) is calculated by dividing t' for a dose by t' for the very first dose. The dose is admitted after 60 s of baseline collection.

the adsorption experiment. During cooling, a dynamic vacuum (1×10^{-6} Torr) was constantly maintained.

Some typical adsorption data are presented in Fig. 1. Figure 1(a) shows three thermograms demonstrating the changes in the heat evolution dynamics and the decrease in the integrated area with increasing coverage. Figure 1(b) presents the corresponding normalized pressure response curves. From the pressure curves, the amount of gas adsorbed and the normalized adsorption parameter (NAP) were calculated. (The NAP represents the time to 90% completion of the adsorption process, normalized by that of the first dose [28].) From this data, the plots of differential heat of adsorption vs. coverage and the adsorption isotherms were obtained.

X-ray diffraction (XRD)

XRD data were obtained using a Rigaku X-ray diffractometer (model 4011B3). The sample was pressed into a pellet at 10000 lbf in^{-2} to align the Grafoil basal planes and to simplify interpretation of the resulting XRD pattern [21]. Average particle size estimates were made using both the "half-height" and "integral-area" methods [29].

Transmission electron microscopy (TEM)

Transmission electron micrographs were obtained using a Philips model 420 scanning transmission electron microscope. Samples were prepared using a method described in detail elsewhere [28]. The micrographs were used to estimate the particle size distribution by counting a statistically significant number of particles. In turn, this distribution was used to estimate the particle dispersion and thus the $O:Rh_s$ ratio [29]. Energy dispersive X-ray analysis was used to verify that the sample consisted of rhodium crystallites supported on the graphite substrate.

RESULTS

Low-temperature reduction

The fresh sample was loaded into the calorimeter pretreatment reactor as described above and treated in hydrogen at 200 °C to reduce the rhodium salt to zerovalent metal. According to the data of previous workers [15,16,30], a fresh silica-supported rhodium sample prepared from $RhCl_3 \cdot xH_2O$ exhibited two temperature programmed reduction (TPR) peaks when treated in hydrogen: one at 95 °C from reduction of Rh_2O_3, and the other at 140 °C from reduction of $RhCl_3$. Hence, it was anticipated that hydrogen treatment at 200 °C would result in full reduction of the Rh–Grafoil sample, whilst

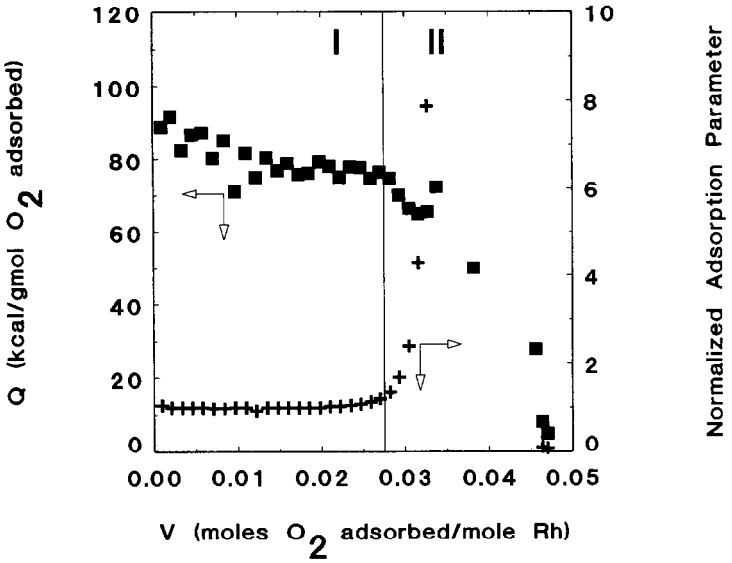

Fig. 2. Differential heat and rate of oxygen adsorption on Rh–Grafoil at 303 K. The two adsorption regions are determined on the basis of changes observed in the adsorption rate as measured by the NAP.

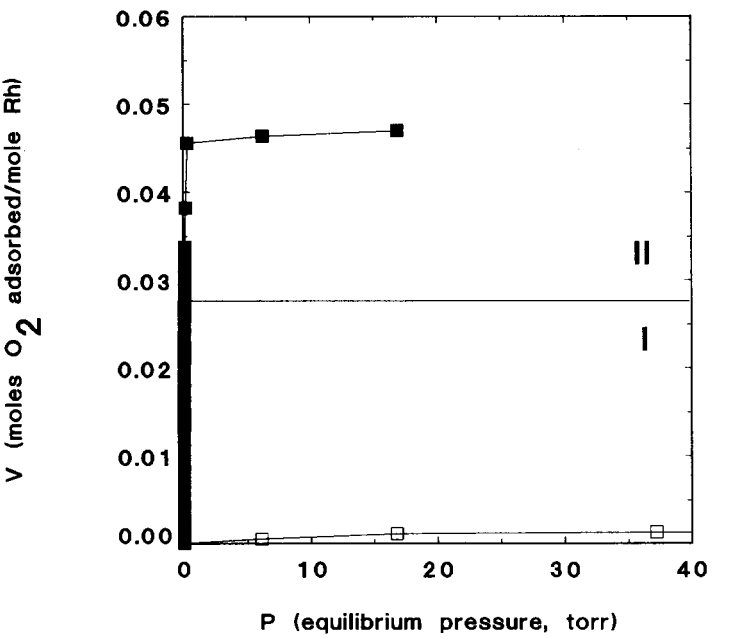

Fig. 3. Adsorption isotherms from oxygen adsorption on Rh–Grafoil at 303 K. The physical adsorption isotherm was measured after evacuation for 4 h at 303 K.

limiting the extent of sintering which is usually associated with high-temperature reduction of Grafoil-supported metal catalysts [21–24].

Figure 2 shows both the differential heat and rate (as measured by the NAP; see Fig. 1 for details) of oxygen adsorption at 303 K on the sample following the low-temperature reduction treatment. Figure 3 presents the corresponding adsorption isotherms. The heat data exhibit significantly more scatter than was apparent in a previous study of oxygen adsorption on Fe–Grafoil [27,28].

For Rh–Grafoil, the chemical adsorption is divided into two regions according to the changes seen in the calculated NAP. In region I, the heats start at values near 90 kcal (g-mol O_2 adsorbed)$^{-1}$, and then fall gradually with increasing coverage until approximately 60% of the ultimate irreversible uptake has been achieved (see Fig. 2). In this region, the rate of adsorption (i.e. the NAP) is virtually constant. In addition, the isotherm (Fig. 3) shows that the uptake of each dose in region I is virtually 100%. In region II, the process changes dramatically. The heats fall off more rapidly with each dose, from about 75 kcal (g-mol O_2)$^{-1}$ to significantly lower values, and the rate of adsorption decreases (i.e. the NAP increases) significantly with each successive dose. This continues until the sample has been passivated and no further chemical adsorption occurs. The chemisorption isotherm shows that the uptake of each dose in region II remains at 100%, until the chemical adsorption process ceases. This behavior is similar to that seen during oxygen adsorption on Grafoil-supported iron microcrystals [27,28]. However, for the present case, the shape of the differential heat profile is very different from that seen for Fe–Grafoil, which showed virtually constant heats through region I, and an approximately linear decrease in heats in region II.

The integral heat of oxygen adsorption on the Rh–Grafoil sample, calculated on the basis of the area of Fig. 2, is approximately 67.0 kcal (g-mol O_2 adsorbed)$^{-1}$ (Table 1). This is substantially higher than the heats of formation of the various phases of rhodium oxide (Rh_2O_3, 47 kcal (g-mol O_2)$^{-1}$; RhO, 45 kcal (g-mol O_2)$^{-1}$; Rh_2O, 48 kcal (g-mol O_2)$^{-1}$) [31].

The only other differential heat of adsorption data available in the literature for oxygen adsorption on rhodium are those of Brennan et al. [32]. They studied oxygen adsorption on an evaporated rhodium thin film in a Beeck-type isoperibol calorimeter. The differential heat data presented in Fig. 2 are significantly lower over the whole range of coverage than seen in the work of Brennan et al. [32].

The sample was removed from the calorimeter and examined by XRD to establish which phases were present. The diffraction pattern is shown in Fig. 4. The XRD data clearly indicate that the only rhodium phase present following the 200 °C reduction and the subsequent oxygen adsorption experiment is f.c.c. rhodium. No contributions from Rh_2O_3 or $RhCl_3$ are

TABLE 1

Differential adsorption data for oxygen adsorption on Rh–Grafoil at 300 K

Reduction temperature (°C)	Integral Q_{ads} (kcal (g-mol O_2)$^{-1}$	Uptake (mol O_2 (mol Rh)$^{-1}$)	Approx. dispersion (Rh_s/Rh) [a]	Approx. O : Rh_s ratio [b]
200	67	0.046	0.13	0.7
400	62	0.014	0.07	0.4

[a] The dispersion was estimated from particle sizes obtained from X-ray line broadening and TEM distributions [29]. The values obtained by the two methods were in excellent agreement.

[b] The O : M_s ratio was calculated on the basis of the measured uptake and the estimated dispersion.

evident in the XRD pattern. Line-broadening calculations provided the particle size estimates shown in Table 2. The average diameters of 93 Å and 80 Å were estimated using the half-height and integral Scherrer methods respectively [29]. Since the former method is more sensitive to larger particles in a distribution, while the latter takes into account all particles, the two can be used to establish the "breadth" of the particle size distribution. In addition, as discussed elsewhere [27,28], for unimodal distributions the "integral" Scherrer method yields a number approximately equal to that calculated using the third moment of the corresponding TEM distribution, whereas the average calculated by the "half-height" method is approximately equivalent to that obtained from the fourth moment of the TEM distribution. Assuming that the particle size distribution in this case has a broad log–normal shape, as may be expected for most Grafoil-supported metal particles [21–24], it is possible to obtain an estimate of the dispersion of the rhodium particles on the basis of the XRD-derived average particle sizes. Using this approach a dispersion of about 13% is estimated for the

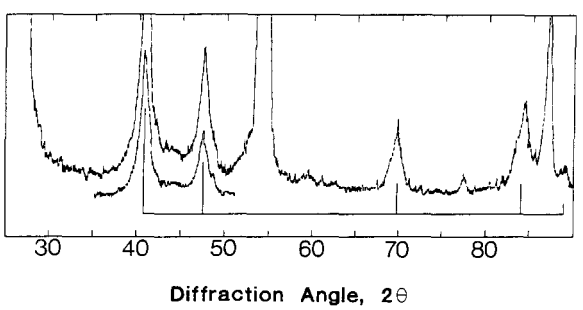

Fig. 4. XRD pattern of Rh–Grafoil collected after 200 °C hydrogen reduction and differential oxygen adsorption at 303 K.

TABLE 2

Estimated average particle sizes of Rh–Grafoil

Reduction temperature (°C)	Technique	Diameter [a]	Estimated average (Å)
200	XRD	$D_{\beta\frac{1}{2}}$	93
		$D_{\beta\frac{1}{2}}$	80
400	XRD	$D_{\beta\frac{1}{2}}$	160
		$D_{\beta\frac{1}{2}}$	147
	TEM	$d1$	91
		$d2$	118
		$d3$	150
		$d4$	169

[a] As defined by Matyi et al. [29].

Rh–Grafoil sample following the 200 °C reduction. This corresponds to an O : Rh_s ratio of approximately 0.7 for the irreversible oxygen uptake measured during the differential adsorption experiment (Table 1).

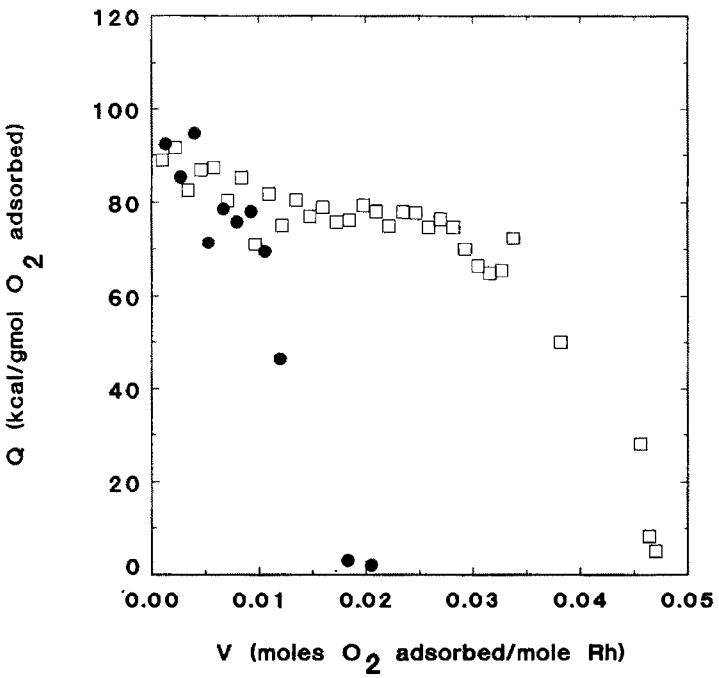

Fig. 5. Differential heat of oxygen adsorption (at 303 K) on Rh–Grafoil following 400 °C hydrogen reduction (filled circles). The data collected following the previous 200 °C reduction are also given for comparison.

High-temperature reduction

The sample was next subjected to a 400 °C hydrogen reduction for 4 h. The data are represented by the filled circles in Fig. 5. The oxygen uptake is seen to decrease, which is a result of sintering.

Following the 400 °C reduction and oxygen adsorption experiment, the sample was again analyzed by XRD. The particle sizes estimated on the basis of X-ray line broadening (Table 2) verify the increase in diameter predicted on the basis of the decreased oxygen uptake. These size estimates were also verified by TEM. A typical micrograph is shown in Fig. 6 and a

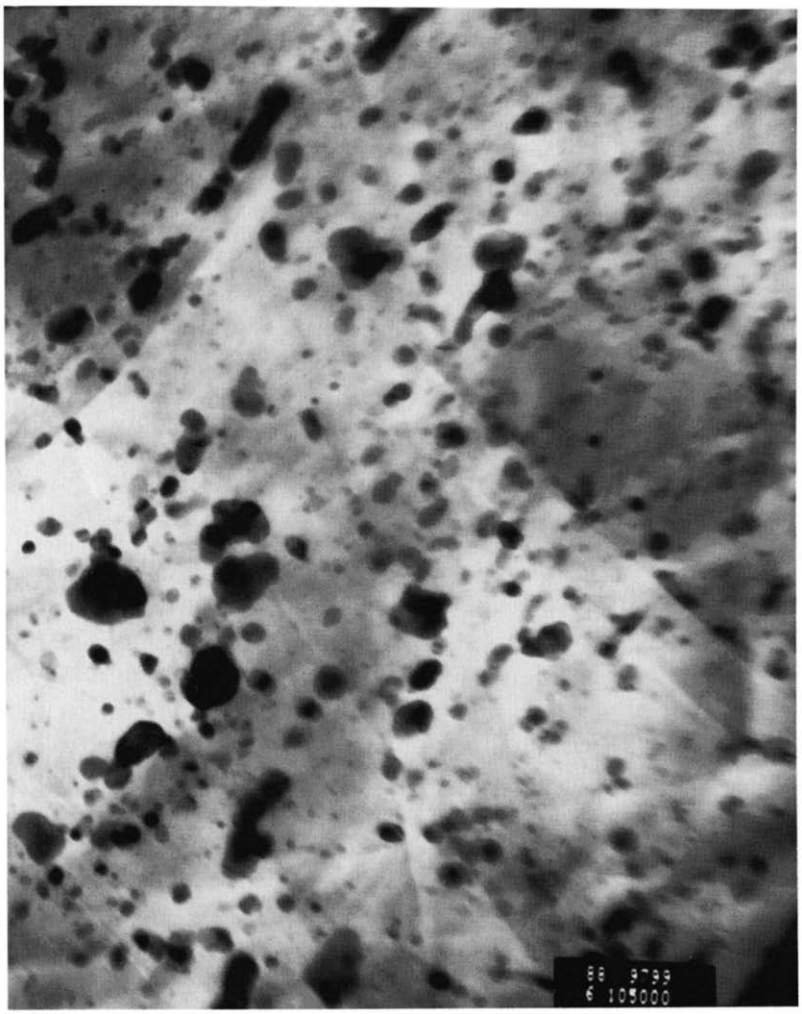

Fig. 6. Transmission electron micrograph of Rh–Grafoil collected after the 400 °C hydrogen reduction and subsequent oxygen adsorption experiment.

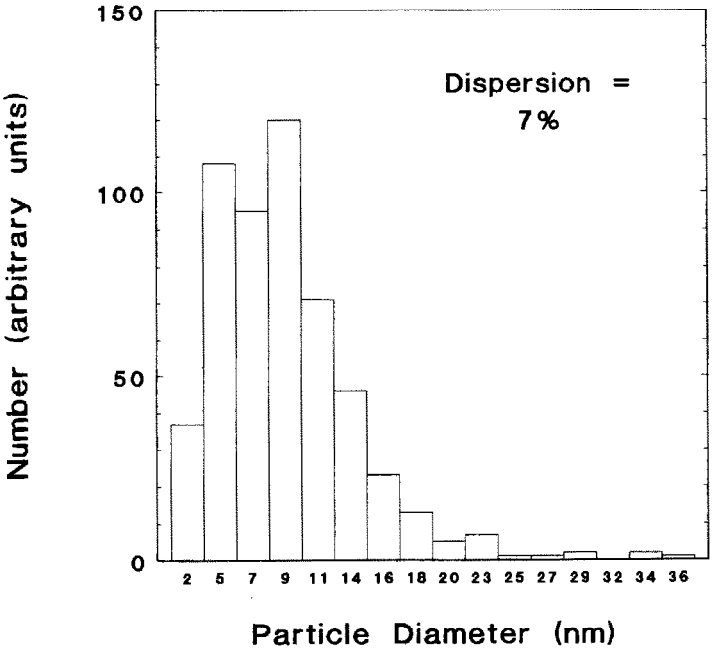

Fig. 7. Particle size distribution estimated by counting particles from the transmission electron micrographs. Approximately 600 particles were counted to generate this distribution.

TEM-derived particle size distribution (estimated by counting approximately 600 particles) is given in Fig. 7. The distribution exhibits the log–normal shape characteristic of Grafoil-supported metal crystallites [21–24]. The average particle diameters estimated on the basis of this distribution are given in Table 2. As stated above, the diameter calculated by the "integral" Scherrer method is roughly the same as the third moment of the TEM-derived distribution, whereas the diameter calculated by the "half-height" Scherrer method is roughly equal to the fourth moment of the distribution. The dispersion calculated on the basis of this distribution is approximately 7% (Table 1). Using this estimate, the $O:Rh_s$ ratio for the sample following the 400 °C reduction is only about 0.4, compared with 0.7 following the 200 °C treatment.

The transmission electron micrographs also clearly indicate the particle growth mechanism. In many of the micrographs, large agglomerates of particles are observed clustering around certain sites on the Grafoil surface. This is consistent with past results which have shown that Grafoil-supported metal particles grow by coalescence along edge or step sites in the graphite crystals [22,23]. This coalescence and growth mechanism invariably results in a log–normal particle size distribution [33,34], as observed in this case.

DISCUSSION

Previous studies of oxygen adsorption on rhodium single crystals and polycrystalline films and foils using ultrahigh vacuum techniques [35–43] have demonstrated that, at room temperature (300 K), the adsorbed oxygen atoms form an ordered layer on the rhodium surface. This layer assumes a (2×1) structure on the Rh(111) crystal face [35] and either a (2×1), $c(2 \times 2)$ or (2×2) structure on the Rh(100) face [42]. These adsorbate surface structures correspond to an approximate chemisorption stoichiometry of 1 : 2 O : Rh_s. The adsorption is rapid, with a sticking probability close to unity [42]. On well-polished, annealed surfaces at low temperature (less than 300 K), only this chemisorbed layer is seen to form. Diffusion of oxygen into the bulk and bulk oxidation are observed only at temperatures above approximately 400 K [35,42].

Previous calorimetric observations by Brennan et al. [32] of room-temperature oxygen adsorption on an evaporated rhodium film have indicated that differential adsorption results in an adsorbed layer with a final O : Rh_s stoichiometry of less than unity (0.84, based on the initial film area). In addition, they measured an integral heat of adsorption of about 76 kcal (g-mol O_2 adsorbed)$^{-1}$, which is significantly higher than the data obtained in this study. Their conclusions, based on these results, were that the adsorption represented true chemisorption of oxygen atoms on the rhodium surface, and that no bulk oxidation occurred. They made similar conclusions for all of the noble Group VIII metals which they studied (rhodium, palladium, platinum). As mentioned previously, the differential heat data measured by these workers are significantly higher over the whole range of coverage than those collected in this work.

There is insufficient evidence available to propose a definitive model of oxygen adsorption on rhodium. However, a few simple assumptions do serve to explain the vast majority of the data. First, it is assumed that the heat and stoichiometry of oxygen adsorption are functions of particle size. In particular, it is suggested that on large particles adsorption occurs primarily on well-defined planes with a well-defined stoichiometry (1 : 2 O : Rh_s) with a relatively high heat of adsorption. In contrast, on small particles, although some adsorption occurs on well-defined planes, a relatively high fraction occurs at 'defect' sites (e.g. edges, corners). The stoichiometry of adsorption at the defect sites tends to be greater than one oxygen atom to two rhodium atoms, and the average heat of adsorption at these sites also tends to be lower.

This model explains all the data collected in this work. For example, the adsorption on small supported rhodium particles (following the 200 °C treatment) is not an equilibrium process. The fluctuations in the measured heat of adsorption with coverage are not consistent with an equilibrium process. These fluctuations are well outside the range of experimental error

of the instrument as determined in previous work with Grafoil-supported iron and iron–rhodium alloy particles [27,28]. In those studies it was found that the maximum 'fluctuation' between points was of the order of ± 2 kcal, or about the height of one of the data points in Fig. 5. Competition for oxygen between small and large particles, which adsorb with different characteristics, could readily lead to this fluctuation-type behavior. As can be seen in Fig. 7, there is a wide particle size distribution. It is suggested that there is intraparticle, but not interparticle, equilibrium.

The model can also explain the high oxygen : rhodium surface atom ratio (0.7) for the highly dispersed rhodium (following the 200 °C treatment) and the lower stoichiometry (0.4) for the sintered particles (following the 400 °C treatment). The highly dispersed particle has a relatively large fraction of defect sites at which 'multiple' oxygen adsorptions can take place. The sintered particles behave in a manner closer to that anticipated on the basis of single-crystal studies, which suggest an average surface stoichiometry of 0.5 [35].

The model also explains why the heat of adsorption in this study for the highly dispersed rhodium (200 °C treatment) is lower than that measured in a previous, and reliable, thin-film study [32]. Presumably, the particles in the thin film are larger and thus adsorb oxygen with a higher average heat value.

In addition the model is consistent with previous work which shows that the surface chemistry of rhodium particles is very dependent on particle size. For example, several workers have shown that the stoichiometry of CO adsorption on supported rhodium particles is dependent on particle size [44–48]. It is also known that hydrogen adsorption stoichiometry is dependent on particle size [14–16]. Furthermore, the activity of supported rhodium particles for benzene hydrogenolysis and NO reduction is dependent on particle size [49].

REFERENCES

1 J.C. Schlatter and P.J. Mitchell, Ind. Eng. Chem., Prod. Res. Dev., 19 (1980) 288.
2 C. Wong and R.W. McCabe, J. Catal., 107 (1987) 535.
3 G.M. Nuñez, A.R. Patrignani and A.J. Rouco, J. Catal., 98 (1986) 554.
4 I. Mochida, N. Ikeyama, H. Ishibashi and H. Fujitsu, J. Catal., 110 (1988) 159.
5 W.F. Graydon and M.D. Langan, J. Catal., 69 (1981) 180.
6 T. Iizuka, Y. Tanaka and K. Tanabe, J. Catal., 76 (1982) 1.
7 S. Kesraoui, R. Oukaci and D. Blackmond, J. Catal., 105 (1987) 432.
8 D.N. Belton, Y.-M. Sun and J.M. White, J. Catal., 102 (1986) 338.
9 D.N. Belton, Y.-M. Sun and J.M. White, J. Am. Chem. Soc., 106 (1984) 3059.
10 H.F.J. van't Blik and R. Prins, J. Catal., 99 (1986) 239.
11 J.H. Craig, Jr., Appl. Surf. Sci., 17 (1984) 379.
12 A. Bertucco and C.O. Bennett, Appl. Catal., 35 (1987) 329.
13 A. Crucq, G. Lienard, L. Degols and A. Frennet, Appl. Surf. Sci., 17 (1983) 79.
14 B.J. Kip, F.B.M. Duivenvoorden, D.C. Kroningsberger and R. Prins, J. Catal., 105 (1987) 26.

15 J.C. Vis, H.F.J. van't Blik, T. Huizinga, J. van Grondelle and R. Prins, J. Catal., 95 (1985) 333.
16 J.C. Vis, H.F.J. van't Blik, T. Huizinga and R. Prins, J. Mol. Catal., 25 (1984) 367.
17 S. Fuentes, A. Vazquez, R. Silva, J.G. Perez-Ramirez and M.J. Yacaman, J. Catal., 111 (1988) 353.
18 P. Bosch, D. Acosta, J. Zenith, D.M. Nicolson and B.C. Gates, J. Mol. Catal., 31 (1985) 73.
19 S. Chakraborti, A.K. Datye and N.J. Long, J. Catal., 108 (1987) 444.
20 T. Wang and L. Schmidt, J. Catal., 70 (1981) 187.
21 N.-L. Wu and J. Phillips, Surf. Sci., 184 (1987) 463.
22 J. Phillips, B. Clausen and J.A. Dumesic, J. Phys. Chem., 84 (1980) 1814.
23 J. Phillips and J.A. Dumesic, Appl. Surf. Sci., 7 (1981) 215.
24 S.-C. Lin and J. Phillips, J. Appl. Phys., 58 (1985) 1943.
25 M. Bretz, J.G. Dash, D.C. Hickernell, E.O. McLean and O.E. Vilches, Phys. Rev. A, 8 (1973) 1589.
26 J.K. Kjems, L. Passell, H. Taub, J.G. Dash and A.D. Novao, Phys. Rev. B, 13 (1976) 1446.
27 R.R. Gatte and J. Phillips, Langmuir, accepted.
28 R.R. Gatte, Ph.D. Thesis, Pennsylvania State University, 1988.
29 R.J. Matyi, L.H. Schwartz and J.B. Butt, Catal. Rev.-Sci. Eng., 29 (1987) 41.
30 H.F.J. van't Blik and J.W. Niemantsverdriet, Appl. Catal., 10 (1984) 155.
31 J.P. Coughlin, Bulletin 542, U.S. Bureau of Mines, U.S. Government Printing Office, Washington DC, 1954.
32 D. Brennan, D.O. Hayward and B.M.W. Trapnell, Proc. R. Soc. London, Ser. A, 256 (1960) 81.
33 C.G. Granqvist and R.A. Buhrman, J. Catal., 42 (1976) 477.
34 C.G. Granqvist and R.A. Buhrman, J. Appl. Phys., 47 (1976) 2200.
35 D.G. Castner and G.A. Somorjai, Appl. Surf. Sci., 6 (1980) 29.
36 D.G. Castner, B.A. Sexton and G.A. Somorjai, Surf. Sci., 71 (1978) 519.
37 D.G. Castner and G.A. Somorjai, Surf. Sci., 83 (1979) 60.
38 P.A. Thiel, J.T. Yates and W.H. Weinberg, Surf. Sci., 82 (1979) 22.
39 J.T. Yates, P.A. Thiel and W.H. Weinberg, Surf. Sci., 82 (1979) 45.
40 J.T. Grant and T.W. Haas, Surf. Sci., 21 (1970) 76.
41 V.V. Gorodetskii, B.E. Nieuwenhuys, W.M.H. Sachtler and G.K. Boreskov, Appl. Surf. Sci., 7 (1981) 355.
42 T. Matsushima, J. Catal., 85 (1984) 98.
43 N. van Hieu and J.H. Craig, Jr., Appl. Surf. Sci., 20 (1984) 121.
44 D.J.C. Yates and J.H. Sinfelt, J. Catal., 8 (1967) 348.
45 E.B. Prestridge, G.H. Via and J.H. Sinfelt, J. Catal., 50 (1977) 115.
46 M. Kobayashi and J. Shirasaki, J. Catal., 28 (1973) 289.
47 M. Kobayashi and J. Shirasaki, J. Catal., 32 (1974) 254.
48 C.R. Guerra and J.H. Schulman, Surf. Sci., 7 (1967) 229.
49 H.C. Yao, Y.F. Yu Yao and K. Otto, J. Catal., 56 (1979) 21.